



Research article

The polycaprolactone and silk fibroin nanofibers with Janus-structured sheaths for antibacterial and antioxidant by loading Taxifolin

Kun Jiao^a, Maolei Sun^{b,c}, Wenyuan Jia^{c,d}, Yun Liu^{a,c}, Shaoru Wang^{c,e}, Yuheng Yang^{c,d}, Zhihui Dai^{c,e}, Liping Liu^{c,e}, Zhiqiang Cheng^{c,f}, Guomin Liu^{c,d}, Yungang Luo^{a,*}

^a The First Hospital of Jilin University, Changchun, 130000, China

^b Department of Stomatology, The Second Hospital of Jilin University, Changchun, 130000, China

^c Scientific and Technological Innovation Center of Health Products and Medical Materials with Characteristic Resource of Jilin Province, Changchun, 130000, China

^d Department of Orthopedics, The Second Hospital of Jilin University, Changchun, 130000, China

^e Department of Prosthodontics, Hospital of Stomatology, Jilin University, Changchun, 130000, China

^f College of Resources and Environment, Jilin Agriculture University, Changchun, 130000, China

ARTICLE INFO

Keywords:

Nanocomposites
Electrospinning
Janus
Core-shell
Taxifolin
Biomaterials

ABSTRACT

Electrospinning is a widely recognized method for producing Janus or core-shell nanofibers. In this study, nanofibrous membranes were fabricated through co-axial electrospinning utilizing polycaprolactone (PCL) and silk fibroin (SF) as the Janus shell, and taxifolin (TAX) and SF as the core. The resulting nanofibers had diameters of 816 ± 161 nm and core diameters of 73 ± 5 nm. The morphology and properties of the PCL-SF@SF/TAX nanofibers were subsequently analyzed. The results demonstrated that the nanofibrous membranes achieved physical and chemical characteristics potential for tissue engineering and drug delivery. Specifically, the membranes exhibited a Young's modulus of 9.64 ± 0.29 MPa, a water contact angle of $79.1 \pm 1.3^\circ$, and a weight loss of 17.3 ± 1.0 % over a period of 28 days. The incorporation of TAX endowed the membranes with antibacterial properties, effectively combating *Escherichia coli* and *Staphylococcus aureus*. Furthermore, the membranes demonstrated antioxidant capabilities, with a DPPH radical scavenging efficiency of 38.5 ± 5.6 % and a Trolox-equivalent antioxidant capacity of 0.24 ± 0.01 mM. The release of the antioxidant was sustained over 28 days, following first-order release kinetics. The nanofibrous membranes, referred to as PSST, exhibit promising potential for use as biomaterials, characterized by their antibacterial activity, antioxidant and cytocompatibility.

1. Introduction

For the sophisticated creation of fiber materials across various scientific domains, electrospinning has risen to prominence as an essential technological innovation [1]. In the domain of biomedicine, the transformative potential of electrospinning is evident, with

* Corresponding author.

E-mail address: luoyg@jlu.edu.cn (Y. Luo).

<https://doi.org/10.1016/j.heliyon.2024.e33770>

Received 21 April 2024; Received in revised form 24 June 2024; Accepted 26 June 2024

Available online 27 June 2024

2405-8440/© 2024 Published by Elsevier Ltd. This is an open access article under the CC BY-NC-ND license (<http://creativecommons.org/licenses/by-nc-nd/4.0/>).

applications spanning innovative drug delivery systems, the repair and replacement of tissues via engineering, and the development of cutting-edge biosensors [2]. Multifluid electrospinning has emerged as a groundbreaking approach, enabling the production of innovative, high-tech fibers with a multitude of functionalities [3]. Janus fibers epitomize a unique bi-functionality, with each of their two sides showcasing a singular set of intrinsic attributes [4].

In the realm of bio-medical applications, biodegradable and resorbable polymers—highlighted by polycaprolactone (PCL) and poly (α -L-glutamic acid)—have been integral to advancements in tissue engineering, drug delivery systems, wound healing, scaffold construction, and the development of surgical sutures [5]. The robust properties of PCL, an FDA-approved polyester, which include remarkable strength, tunable biodegradability, non-cytotoxicity, and biocompatibility, have solidified its role in a variety of applications in the current tissue engineering domain [6,7]. As a result, PCL possesses exceptional toughness, mechanical strength, and biocompatibility, it has been employed in tissue-engineering scaffolds to repair skin, vascular tissues, and bone [8]. It is a semi-crystalline aliphatic polyester that breaks down in the body into repeating units of one ester group and five methylene groups, which have non-cytotoxic effects [9]. Furthermore, cell adhesion and proliferation are generally inhibited by PCL hydrophobicity [8]. Silk fibroin (SF), with its impressive elasticity and reduced potential for immunogenic reactions, is a biopolymer that has become a staple in tissue engineering applications [10]. Glycine, Alanine, and Serine, the amino acid sequence of SF, provide functional groups that encourage cell adhesion [11]. However, membranes prepared with SF lack sufficient mechanical strength, which limit its application. In order to create nanofiber membranes with adequate mechanical qualities, appropriate hydrophilicity, and suitable degradability, PCL and SF were combined. With pharmacological activities that include anti-inflammatory, antioxidant, anti-fibrotic, and immunological regulatory capabilities, taxifolin is a significant naturally occurring dihydroflavone that is being extensively researched and utilized in food, medicine, and other health-related goods [12]. Therefore, in order to get antioxidant and antibacterial characteristics, we provoked Taxifolin into the nanofiber.

Recent years have seen a major advancement in electrospinning technology-based strategies for biomedical applications [13]. The capacity of electrospinning technology to create fibers with nanoscale dimensions that have the potential to closely resemble the structure and functions of the extracellular matrix has drawn attention [14,15]. The prevalence of research in uniaxial electrospinning, shell-core nanofibers, and Janus nanofibers contrasts with the dearth of studies on Janus and shell-core fibers from co-axial electrospinning, indicating an area ripe for exploration [16]. Utilizing electrospinning, it becomes a simple and efficient task to produce nanofibrous architectures that parallel the characteristics of the native extracellular matrix [17]. In biomedical applications, the shell material of nanofibers is strategically employed to modulate the burst release kinetics of embedded particles, thereby enhancing their sustained and controlled release over an extended period. Meanwhile, the core material serves as a protective reservoir for encapsulating sensitive bioactive agents such as growth factors, proteins, and medications [18]. Electrospinning is used in research to prepare nanofibers with specified structural properties for use in innovative medication delivery systems [19,20]. By carefully regulating drug release behavior, these nanofibers not only increase drug solubility and bioavailability but also improve therapeutic efficacy [21–23].

In the present study, we successfully fabricated core-shell nanofiber membranes via the technique of coaxial electrospinning. These membranes feature a PCL-SF Janus shell and a TAX/SF core, endowing them with a triad of desirable properties: antibacterial activity, antioxidant capacity, and cytocompatibility. The preparation of the nanofiber membrane that combines the positive cell adhesion characteristics of SF with the strong mechanical qualities of PCL is the goal of this work. Moreover, by adding TAX, to impart specific antibacterial and antioxidant characteristics, promising for use in tissue engineering and drug delivery.

2. Experimental

2.1. Materials

PCL with a molecular weight of 80,000, hexafluoroisopropanol (HFIP), and dichloromethane (CH_2Cl_2) were sourced from Aladdin Biochemical Technology Co., Ltd, located in Shanghai, China. SF was procured from Simatech Incorporation, based in Soochow, China. The National Institutes for Food and Drug Control of China supplied TAX, identified by batch numbers 111,816-201,102, and characterized by a 98.0 % purity level. For cell culture, DMEM and a combination of penicillin and streptomycin were acquired from Hyclone, situated in Logan, Utah, USA. Fetal bovine serum (FBS) was secured from Biological Industries, a company in Cromwell, Connecticut, USA. Additionally, the Calcein-AM/PI viability stain kit and the CCK-8 cell proliferation assay kit were both supplied by BestBio, a company in Shanghai, China.

2.2. Fabrication of PSS and PSST nanofiber membranes

Solution a was created by dissolving PCL (8.6 wt%) in HFIP. Solution b was created by dissolving SF (6.8 wt%) in HFIP. Solution c was created by dissolving SF (5.2 wt%) in HFIP and CH_2Cl_2 (10:1 wt percent). The solution c, now known as solution d, had TAX (1.7 wt%) added to it. At 37 °C, the solutions were agitated all night. The sheath solution was then combined with solutions a and b (1:1 v/v) and injected into a 5 mL syringe attached to the external spinneret. An internal spinneret-mounted 5 mL syringe was filled with either solution c or d, which was named PSS or PSST. The tip-to-collector distance was 15 cm with 18 kV voltage applied, the inner shaft feed rate was 0.6 mL h^{-1} through the 21-G needle and the outer shaft feed rate was 2 mL h^{-1} through the 16-G needle for the coaxial electrospinning process, which were collected on a grounded aluminum plate completely covered by aluminum foil. The electrospinning was carried out at room temperature and ~40 % humidity.

2.3. Surface and structure characterization

The surface structures of both PSS and PSST were examined through SEM (model SHIMADZU X-550, operating at 15.0 kV) following gold coating, and TEM (JOEL JEM-201). The presence of functional groups in the nanofibers was identified with an FTIR spectrometer (model FTIR-650). Wettability of the nanofibers was measured using a contact angle meter (SL2000KS). For the degradation test, nanofibers, averaging 100 mg in mass, were immersed in 5 mL of artificial saliva, with weight measurements taken at intervals of 1, 3, 7, 14, 21, and 28 days. In a separate experiment, PSST samples, weighing approximately 50 mg, were immersed in 5 mL of PBS at a temperature of 37 °C. At regular intervals, 2 mL of the solution were extracted and replaced with an equal volume of fresh PBS. The Taxifolin content in the samples was quantified using HPLC, with a calibration curve employed to ensure the accuracy of the measurements.

2.4. Antibacterial assay in vitro

The nanofiber was exposed to a 5 mL solution of bacteria, with a concentration of 1×10^7 CFU per milliliter. Following a 12-h incubation period, a 500 μ L aliquot from each sample group was collected and diluted to a factor of 1×10^7 . This diluted sample was spread evenly across an agar surface, also in a volume of 500 μ L. After a subsequent 24-h incubation at a temperature of 37 °C, bacterial colonies were observed. The study involved the separate cultivation of two distinct bacteria: the gram-negative *Escherichia coli* and the gram-positive *Staphylococcus aureus*. Both were grown in Luria-Bertani (LB) broth at a constant temperature of 37 °C.

2.5. Antioxidant activity

The membranes' antioxidant potential was evaluated by examining their ability to neutralize the DPPH radical. For this, a precise amount of 30 mg of the membranes was mixed with a 0.039 mg/mL concentration of DPPH solution, totaling 2 mL, and the mixture was kept in darkness for a duration of 30 min. The level of absorbance was then recorded at a wavelength of 517 nm, employing a UV-vis spectrophotometer. The efficiency of the DPPH radical scavenging was determined by the equation: Scavenging rate (%) = $(A_0 - A)/A_0 \times 100$, where A_0 is the absorbance of the control and A is the absorbance of the sample under test. Additionally, the membranes' overall antioxidant capacity was gauged using the ABTs assay, strictly adhering to the protocol provided by the assay's supplier. In this process, 30 mg of the membranes were blended with the ABTs reagent and allowed to react at ambient temperature for a period ranging from 2 to 6 min. The optical density was subsequently measured at 734 nm using a microplate reader, facilitating the computation of the membranes' total antioxidant capacity through the creation of a calibration curve.

2.6. Biocompatibility in vitro

Discs of fibrous membranes, each 10 mm in diameter, were prepared and subjected to a 12-h ultraviolet disinfection process. The RAW264.7 cells were grown in DMEM enriched with 10 % FBS and maintained in a controlled environment at 37 °C with 5 % CO₂. To assess the compatibility of the materials with living cells, a seeding density of 5×10^3 RAW264.7 cells per well was applied onto the fibrous membranes in a 96-well format, and their growth was monitored over 24 h using the CCK-8 assay. The assay involved the addition of a 10 % volume fraction of CCK-8 reagent to the culture medium, followed by a 1-h incubation under the same atmospheric

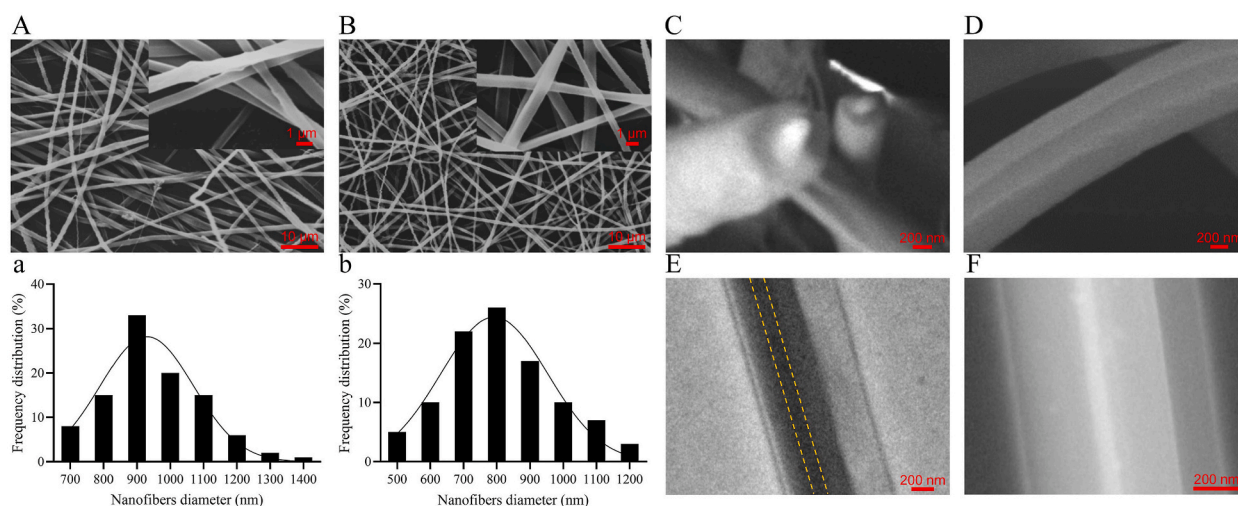


Fig. 1. (A and B) SEM images of PSS and PSST nanofibrous membranes. (a and b) The image of diameter distribution. (C) SEM images of the cross-section of the PSST nanofibrous membranes. (D) SEM images of the PSST nanofibrous membranes after soaking in PBS for 14 days. (E) TEM image of PSST nanofiber. (F) STEM image of PSST nanofiber.

conditions. The resulting absorbance was measured at 450 nm with a Bio-Rad microplate reader, and the relative cell viability was determined using the formula: Cell viability (%) = OD value of sample/OD value of control \times 100.

Furthermore, the nanofibers' impact on cell survival was examined using a calcein-AM/PI staining method. After allowing the cells to grow for 24 h, they were exposed to the staining solution for 15 min at 37 °C in darkness. The stained cells were then examined under a fluorescence microscope, where viable cells displayed green fluorescence and non-viable cells exhibited red fluorescence.

2.7. Statistical analysis

The study employed a fully randomized design with a single variable and triplicate measurements. The hypothesis testing was conducted in accordance with this design, assessing the differences in treatment means via one-way ANOVA. GraphPad Prism 9 was utilized for the statistical computations.

3. Results and discussion

3.1. Morphology of PSS and PSST nanofibrous membranes

SEM images of PSS and PSST nanofibrous membranes (Fig. 1A and B) showed the nanofibrous membranes displayed a three-dimensional network with high porosity, and the mean diameters of PSS and PSST were 951 ± 152 nm and 816 ± 161 nm (Fig. 1a and b), which was similar to the study of Zhou et al. [24]. PSST nanofibers with core-shell structured in SEM image of the cross-section of the nanofibers (Fig. 1C), and with the PCL Janus-structured sheaths with a grooved, which was located the SF core and another SF Janus-structured sheaths, in SEM image of the nanofibers after soaked in PBS 14 days (Fig. 1D). The nanofibers were separated into three portions in TEM image (Fig. 1E) and STEM image (Fig. 1F), in which the diameters of the core was 73 ± 5 nm.

The single-fluid blending electrospinning is facile to encapsulate a certain drug with a high encapsulation efficiency. As shown in Fig. 2A, PCL demonstrates absorbance peaks at 1731 cm^{-1} denoted the C=O carbonyl ester stretching [25]. In SF, the peaks at 1653 cm^{-1} (C=O stretching vibration) and 1541 cm^{-1} (N-H vibration) were due to random coil structure [26]. In PSS and PSST, the peaks at 1731 cm^{-1} , 1653 cm^{-1} and 1541 cm^{-1} were observed. The hydrogen bonding and benzene ring structure were indicated by the peaks between 2700 cm^{-1} – 3800 cm^{-1} in TAX [27], but not observable in PSST, which indicated the TAX loaded and intermolecular hydrogen bond formation due to the phenolic hydroxyl group in TAX and the free amino groups and free carboxyl groups in SF.

For nanofibers to be able to withstand the stress brought on by tissue engineering, they must possess a sufficient level of mechanical strength. The stress and strain curve of manufactured PSS and PSST is shown in Fig. 2B. By examining the average ultimate tensile stress, ultimate tensile strain, and Young's modulus of the nanofibers, this study investigated their mechanical characteristics. A highly porous scaffold made of polymer will frequently display early elastic behavior, which means it will bend before breaking. The tensile stress, tensile strain and Young's modulus of PSS and PSST are 5.35 ± 0.37 MPa, $12.63 \pm 0.46\%$, and 5.67 ± 0.43 MPa, respectively, and 4.62 ± 0.30 MPa, $13.85 \pm 0.39\%$ and 9.64 ± 0.29 MPa, which are similar to Bio-Gide® [28].

The surface wettability of a biomaterial is an important component in tissue engineering because it affects the level of cellular

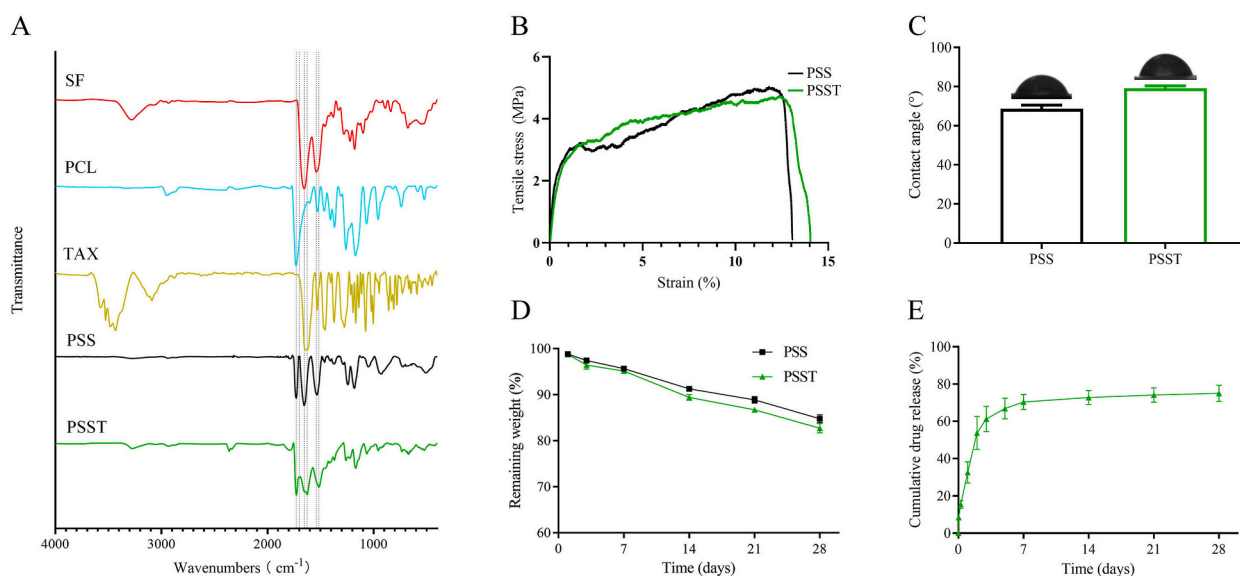


Fig. 2. (A) The FTIR spectra of SF, PCL, TAX, PSS, PSST membranes. (B) The mechanical properties of PSS and PSST membranes. (C) Water contact angles of PSS and PSST membranes. (D) The degradation profiles of the PSS and PSST membranes. (E) Cumulative TAX release from the PSST membranes.

adhesion, the dispersion of cells inside nanofibers, and the rate of tissue regeneration. Fig. 2C displays the water contact angle image of electrospun mats possessing values $68.6 \pm 1.9^\circ$ and $79.1 \pm 1.3^\circ$, even increased after TAX loaded, which indicates that PSS and PSST are suitable for stimulating cell growth and supports studies had demonstrated that for cell adhesion and proliferation, a contact angle value less than 90° is preferable.

The mass of the PSS and PSST is reduced by $15.2 \pm 0.8\%$ and $17.3 \pm 1.0\%$ in 28 days (Fig. 2D), which is necessary for tissue regeneration. Drug-loaded nanofibrous membranes demonstrated an excellent drug release ratio and rate. Fig. 2D shows how the addition of TAX regulated the nanofibrous membranes' drug release profile trend and stopped the first "burst" release. There was an acute release of TAX in the first two days from PSST. Afterwards, the release rate gradually slowed down during days 2–28. Four simulation models were fitted to intuitively evaluate the release kinetics of TAX. The fitting equation in Table 1 supported the fact that the release of TAX in PSST conformed to the first order release kinetics with 0.97 for R^2 , of which R^2 was 0.67, 0.87 and 0.93 for zero-order, Higuchi and Ritger-Peppas release kinetics.

3.2. Biocompatibility in vitro

No cytotoxicity is the most basic requirement of biomaterials. After culturing for 24 h, most of the seeded RAW264.7 cells stayed alive (green fluorescence) on the two nanofibers and few dead cells (red fluorescence) were observed in Fig. 3A, using a Calcein-AM/PI double stain kit for the live/dead staining. The results were confirmed by CCK-8 assay, after the RAW264.7 inoculated onto the surfaces of the PSS and PSST nanofibers to investigate the effect of the nanofibers on the cell proliferation for 24 h. Fig. 3B illustrates that there was no significant difference in cell viability between each group, which was similar to the study of Jiang et al. [29].

3.3. Antioxidant activity and antibacterial property of nanofibrous membranes

The antioxidant capacity of the PSS and PSST was determined by *in vitro* DPPH and ABTS assays. As shown in Fig. 3C, the DPPH clearance rate of PSS and PSST was $4.6 \pm 2.1\%$ and $38.5 \pm 5.6\%$. In Fig. 3D, the Trolox-equivalent antioxidant capacity of PSS and PSST was 0.03 ± 0.00 mM and 0.24 ± 0.01 mM. With the addition of TAX, the antioxidant capacity of nanofibrous membranes was improved. TAX can neutralize these reactive oxidizing species by donating electrons, with 3', 4' -OH, which had strong antioxidant activity [30].

The antibacterial activity of PSS and PSST electrospun fiber membranes single-loaded with TAX against *Staphylococcus aureus* and *Escherichia coli* is depicted optically in Fig. 3E. Compared with the control group, PSS had slight antibacterial activity ($11.9 \pm 4.4\%$ and $7.1 \pm 2.2\%$), while PSST had obvious antibacterial activity ($44.4 \pm 2.9\%$ and $53.7 \pm 2.3\%$). The phenolic hydroxyl of TAX could bind to the phospholipid bilayer of bacteria and the amino and carboxyl groups in bacterial membrane proteins and disrupt the integrity of the bacterial membrane [31]. The biomaterial with strong antibacterial properties shows great potential for medical implant materials in clinic application [32]. This efficient antibacterial property of the TAX-loaded nanofibers showed their great potential for bacterial disinfection biomedicine.

To fully utilize the antimicrobial and antioxidant properties of PSST, our current main research goal is to apply it to tissue engineering and other fields. In terms of cell experiments, we have made some progress, although this is not stated in the study. Additionally, animal experiments are the next major experimental directions of this study. Our current proposal is to use it for skin repair (NIH/3T3 cells) [33] and osteogenesis (MC3T3-E1) [34] and to conduct additional studies related to antimicrobials in the future. To fully utilize the capabilities of nanofibers and accomplish a variety of applications in diverse medical domains, additional medications can be added to the PCL and SF of the nanofiber shells, such as risedronate [35] for osteoporosis and tacrolimus [36] for immunomodulatory.

4. Conclusion

Through the application of co-axial electrospinning, we successfully fabricated PSST Janus shell-core nanofibrous membranes. SEM analysis disclosed their porous nature, and both cross-sectional SEM and TEM images underscored the nanofibers' distinctive shell-core and Janus-structured sheaths. The presence of PCL, SF, and TAX was validated by FTIR spectroscopy. Overall, this research highlights the significant potential of PSST nanofibrous membranes for applications in biomaterials, specifically in antibacterial and antioxidant capacities for tissue engineering.

Table 1

Kinetic models for the release of TAX from PSST nanofibers (M_t represents the cumulative drug release at time t).

stimulation model	equation	R^2
zero-order	$M_t = 0.03t + 0.16$	0.67
first-order	$M_t = 0.72(1 - e^{-0.88t})$	0.97
Higuchi	$M_t = 0.16t^{1/2} + 0.09$	0.87
Ritger-Peppas	$M_t = 0.30t^{0.32}$	0.93

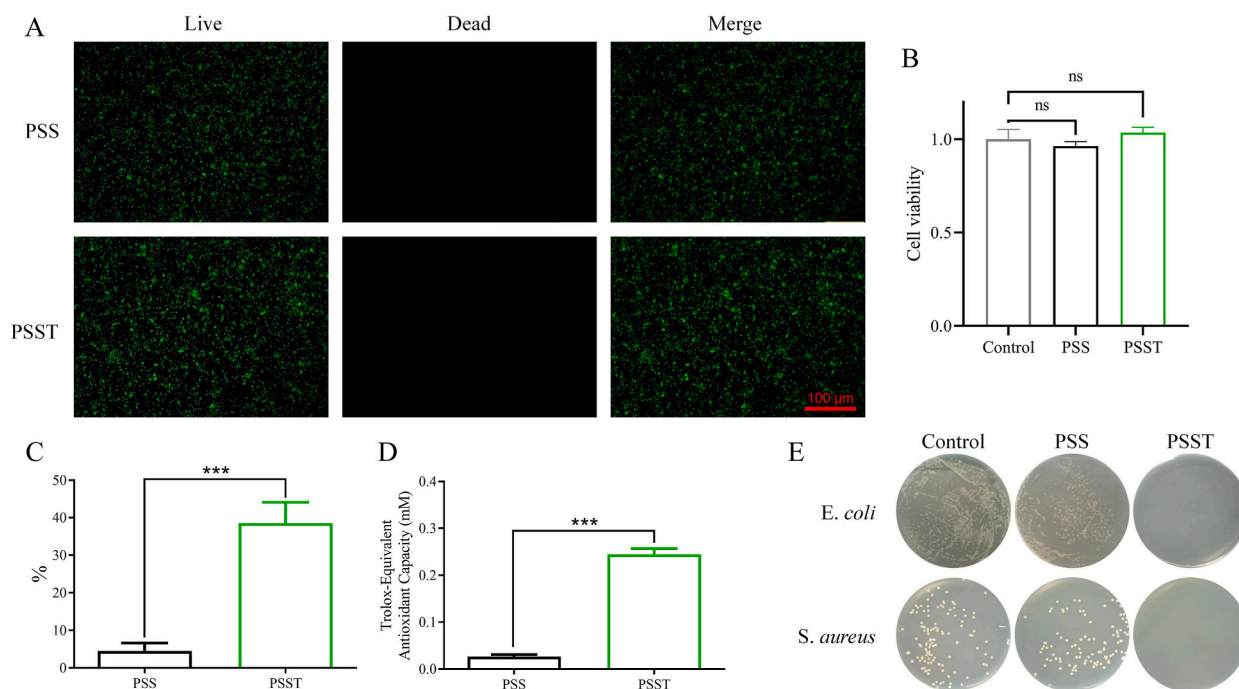


Fig. 3. (A) Fluorescent staining of live/dead of RAW264.7 on PSS and PSST nanofibers at day 1. (B) Activity of RAW264.7 on the surface of the PSS and PSST nanofibers measured by CCK-8 assay on day 1. (C) The DPH clearance rate of PSS and PSST. (D) The Trolox-equivalent antioxidant capacity of PSS and PSST. (E) Agar plate images for *E. coli* and *S. aureus* treated with the PSS and PSST nanofibers. All statistical data are represented as mean \pm SD ($n = 3$; $^{ns}P > 0.05$ and $^{***}P < 0.001$).

Data availability statement

Data will be made available on request.

CRediT authorship contribution statement

Kun Jiao: Writing – original draft, Methodology, Formal analysis, Conceptualization, Investigation. **Maolei Sun:** Writing – review & editing, Validation. **Wenyuan Jia:** Investigation, Formal analysis, Data curation. **Yun Liu:** Investigation, Formal analysis. **Shaoru Wang:** Visualization. **Yuheng Yang:** Software, Data curation. **Zhihui Dai:** Validation, Investigation. **Liping Liu:** Data curation. **Zhiqiang Cheng:** Validation, Investigation. **Guomin Liu:** Supervision, Project administration, Funding acquisition. **Yungang Luo:** Supervision, Project administration, Funding acquisition, Conceptualization, Writing – review & editing.

Declaration of competing interest

The authors declare that they have no known competing financial interests or personal relationships that could have appeared to influence the work reported in this paper.

Acknowledgments

This work was supported by the Department of Science and Technology of Jilin Province [grant numbers 20220204124YY, 20220508084RC, 20230204115YY].

References

- [1] X. Xu, M. Zhang, H. Lv, Y. Zhou, Y. Yang, D.-G. Yu, Electrospun polyacrylonitrile-based lace nanostructures and their Cu(II) adsorption, *Sep. Purif. Technol.* 288 (2022) 120643, <https://doi.org/10.1016/j.seppur.2022.120643>.
- [2] S. Kang, K. Zhao, D.-G. Yu, X. Zheng, C. Huang, Advances in biosensing and environmental monitoring based on electrospun nanofibers, *Adv. Fiber Mater.* 4 (3) (2022) 404–435, <https://doi.org/10.1007/s42765-021-00129-0>.
- [3] K. Zhao, Z.-H. Lu, P. Zhao, S.-X. Kang, Y.-Y. Yang, D.-G. Yu, Modified tri-axial electrospun functional core-shell nanofibrous membranes for natural photodegradation of antibiotics, *Chem. Eng. J.* 425 (2021) 131455, <https://doi.org/10.1016/j.cej.2021.131455>.
- [4] P.M. Silva, S. Torres-Giner, A.A. Vicente, M.A. Cerqueira, Management of operational parameters and novel spinneret configurations for the electrohydrodynamic processing of functional polymers, *Macromol. Mater. Eng.* 307 (5) (2022) 2100858, <https://doi.org/10.1002/mame.202100858>.

- [5] S. Hassanajili, A. Karami-Pour, A. Oryan, T. Talei-Khozani, Preparation and characterization of PLA/PCL/HA composite scaffolds using indirect 3D printing for bone tissue engineering, *Mater. Sci. Eng. C* 104 (2019) 109960, <https://doi.org/10.1016/j.msec.2019.109960>.
- [6] N. Kong, H. Yang, R. Tian, G. Liu, Y. Li, H. Guan, Q. Wei, X. Du, Y. Lei, Z. Li, R. Cao, Y. Zhao, X. Wang, K. Wang, P. Yang, An injectable self-adaptive polymer as a drug carrier for the treatment of nontraumatic early-stage osteonecrosis of the femoral head, *Bone Res* 10 (1) (2022) 28, <https://doi.org/10.1038/s41413-022-00196-y>.
- [7] Y. Al-Hadeethi, A. Nagarajan, S. Hanuman, H. Mohammed, A.M. Vetekar, G. Thakur, L.N.M. Dinh, Y. Yao, E.M. Mkawi, M.A. Hussein, V. Agarwal, M. Nune, Schwann cell-matrix coated PCL-MWCNT multifunctional nanofibrous scaffolds for neural regeneration, *RSC Adv.* 13 (2) (2023) 1392–1401, <https://doi.org/10.1039/d2ra05368c>.
- [8] A. Bharadwaz, A.C. Jayasuriya, Recent trends in the application of widely used natural and synthetic polymer nanocomposites in bone tissue regeneration, *Mater. Sci. Eng. C* 110 (2020) 110698, <https://doi.org/10.1016/j.msec.2020.110698>.
- [9] X. Yao, L. Zhan, Z. Yan, J. Li, L. Kong, X. Wang, H. Xiao, H. Jiang, C. Huang, Y. Ouyang, Y. Qian, C. Fan, Non-electric bioelectrical analog strategy by a biophysical-driven nano-micro spatial anisotropic scaffold for regulating stem cell niche and tissue regeneration in a neuronal therapy, *Bioact. Mater.* 20 (2023) 319–338, <https://doi.org/10.1016/j.bioactmat.2022.05.034>.
- [10] A. Kopp, R. Smeets, M. Gosau, N. Kroger, S. Fuest, M. Kopf, M. Kruse, J. Krieger, R. Rutkowski, A. Henningsen, S. Burg, Effect of process parameters on additive-free electrospinning of regenerated silk fibroin nonwovens, *Bioact. Mater.* 5 (2) (2020) 241–252, <https://doi.org/10.1016/j.bioactmat.2020.01.010>.
- [11] L.J. Bray, K.A. George, D.W. Huttmacher, T.V. Chirila, D.G. Harkin, A dual-layer silk fibroin scaffold for reconstructing the human corneal limbus, *Biomaterials* 33 (13) (2012) 3529–3538, <https://doi.org/10.1016/j.biomaterials.2012.01.045>.
- [12] A.E. Weidmann, Dihydroquercetin: more than just an impurity? *Eur. J. Pharmacol.* 684 (1–3) (2012) 19–26, <https://doi.org/10.1016/j.ejphar.2012.03.035>.
- [13] Y. Li, Q. Meng, S. Chen, P. Ling, M.A. Kuss, B. Duan, S. Wu, Advances, challenges, and prospects for surgical suture materials, *Acta Biomater.* 168 (2023) 78–112, <https://doi.org/10.1016/j.actbio.2023.07.041>.
- [14] C.D. Zhang, X. Yang, L.D. Yu, X.S. Chen, J.K. Zhang, S. Zhang, S.H. Wu, Electrospun polyasparthydrazide nanofibrous hydrogel loading with in-situ synthesized silver nanoparticles for full-thickness skin wound healing application, *Mater. Des.* 239 (2024) 112818, <https://doi.org/10.1016/j.matdes.2024.112818>.
- [15] Y.R. Li, W.W. Zhao, S.J. Chen, H.Y. Zhai, S.H. Wu, Bioactive electrospun nanoyarn-constructed textile dressing patches delivering Chinese herbal compound for accelerated diabetic wound healing, *Mater. Des.* 237 (2024) 112623, <https://doi.org/10.1016/j.matdes.2023.112623>.
- [16] A. Nagarajan, N. Rizwana, M. Abraham, M. Bhat, A. Vetekar, G. Thakur, U. Chakraborty, V. Agarwal, M. Nune, Polycaprolactone/graphene oxide/acellular matrix nanofibrous scaffolds with antioxidant and promyelinating features for the treatment of peripheral demyelinating diseases, *J. Mater. Sci. Mater. Med.* 34 (10) (2023) 49, <https://doi.org/10.1007/s10856-023-06750-2>.
- [17] T. Jiang, D. Kai, S. Liu, X. Huang, S. Heng, J. Zhao, B.Q.Y. Chan, X.J. Loh, Y. Zhu, C. Mao, L. Zheng, Mechanically cartilage-mimicking poly(PCL-PTHF urethane)/collagen nanofibers induce chondrogenesis by blocking NF-kappa B signaling pathway, *Biomaterials* 178 (2018) 281–292, <https://doi.org/10.1016/j.biomaterials.2018.06.023>.
- [18] R. Augustine, A.A. Zahid, A. Hasan, M. Wang, T.J. Webster, CTGF loaded electrospun dual porous core-shell membrane for diabetic wound healing, *Int. J. Nanomed.* 14 (2019) 8573–8588, <https://doi.org/10.2147/IJN.S224047>.
- [19] J. Zhou, Y. Chen, Y. Liu, T. Huang, J. Xing, R. Ge, D.G. Yu, Electrospun medicated gelatin/polycaprolactone Janus fibers for photothermal-chem combined therapy of liver cancer, *Int. J. Biol. Macromol.* 269 (Pt 1) (2024) 132113, <https://doi.org/10.1016/j.ijbiomac.2024.132113>.
- [20] P. Mosallanezhad, H. Nazockdast, Z. Ahmadi, A. Rostami, Fabrication and characterization of polycaprolactone/chitosan nanofibers containing antibacterial agents of curcumin and ZnO nanoparticles for use as wound dressing, *Front. Bioeng. Biotechnol.* 10 (2022) 1027351, <https://doi.org/10.3389/fbioe.2022.1027351>.
- [21] Y. Sun, J. Zhou, Z. Zhang, D.G. Yu, S.W.A. Blich, Integrated Janus nanofibers enabled by a co-shell solvent for enhancing icariin delivery efficiency, *Int. J. Pharm.* 658 (2024) 124180, <https://doi.org/10.1016/j.ijpharm.2024.124180>.
- [22] M. Ghazalian, S. Afshar, A. Rostami, S. Rashedi, S.H. Bahrami, Fabrication and characterization of chitosan-polycaprolactone core-shell nanofibers containing tetracycline hydrochloride, *Colloids Surf., A* 636 (2022), <https://doi.org/10.1016/j.colsurfa.2021.128163>.
- [23] D. Li, M.L. Wang, W.L. Song, D.G. Yu, S.W.A. Blich, Electrospun Janus beads-on-A-string structures for different types of controlled release profiles of double drugs, *Biomolecules* 11 (5) (2021) 635, <https://doi.org/10.3390/biom11050635>.
- [24] J.F. Zhou, T. Yi, Z.Y. Zhang, D.G. Yu, P. Liu, L.Z. Wang, Y.J. Zhu, Electrospun Janus core (ethyl cellulose//polyethylene oxide) @ shell (hydroxypropyl methyl cellulose acetate succinate) hybrids for an enhanced colon-targeted prolonged drug absorbance, *Adv. Compos. Hybrid Mater.* 6 (6) (2023) 189, <https://doi.org/10.1007/s42114-023-00766-6>.
- [25] A. Bhattacharyya, V.N.K. Priya, J.H. Kim, M.R. Khatun, R. Nagarajan, I. Noh, Nanodiomed enhanced mechanical and biological properties of extrudable gelatin hydrogel cross-linked with tannic acid and ferrous sulphate, *Biomater. Res.* 26 (1) (2022) 37, <https://doi.org/10.1186/s40824-022-00285-3>.
- [26] Q. Zhang, L. Shi, H. He, X. Liu, Y. Huang, D. Xu, M. Yao, N. Zhang, Y. Guo, Y. Lu, H. Li, J. Zhou, J. Tan, M. Xing, G. Luo, Down-regulating scar formation by microneedles directly via a mechanical communication pathway, *ACS Nano* 16 (7) (2022) 10163–10178, <https://doi.org/10.1021/acsnano.1c11016>.
- [27] Y. Zhang, J. Yu, X.D. Dong, H.Y. Ji, Research on characteristics, antioxidant and antitumor activities of dihydroquercetin and its complexes, *Molecules* 23 (1) (2018) 20, <https://doi.org/10.3390/molecules23010020>.
- [28] K.R. Zhang, H.L. Gao, X.F. Pan, P. Zhou, X. Xing, R. Xu, Z. Pan, S. Wang, Y.M. Zhu, B. Hu, D.H. Zou, S.H. Yu, Multifunctional bilayer nanocomposite guided bone regeneration membrane, *Matter* 1 (3) (2019) 770–781, <https://doi.org/10.1016/j.matt.2019.05.021>.
- [29] H. Jiang, X. Wang, X. Li, Y. Jin, Z. Yan, X. Yao, W.E. Yuan, Y. Qian, Y. Ouyang, A multifunctional ATP-generating system by reduced graphene oxide-based scaffold repairs neuronal injury by improving mitochondrial function and restoring bioelectricity conduction, *Mater. Today Bio* 13 (2022) 100211, <https://doi.org/10.1016/j.mtbio.2022.100211>.
- [30] M. Fan, G. Chen, Y. Zhang, L. Nahar, S.D. Sarker, G. Hu, M. Guo, Antioxidant and anti-proliferative properties of hagenia abyssinica roots and their potentially active components, *Antioxidants* 9 (2) (2020) 143, <https://doi.org/10.3390/antiox9020143>.
- [31] S. Xu, L. Chang, Y. Hu, X. Zhao, S. Huang, Z. Chen, X. Ren, X. Mei, Tea polyphenol modified, photothermal responsive and ROS generative black phosphorus quantum dots as nanoplatforams for promoting MRSA infected wounds healing in diabetic rats, *J. Nanobiotechnol.* 19 (1) (2021) 362, <https://doi.org/10.1186/s12951-021-01106-w>.
- [32] M. Bao, Y. Liu, X. Wang, L. Yang, S. Li, J. Ren, G. Qin, E. Zhang, Optimization of mechanical properties, biocorrosion properties and antibacterial properties of wrought Ti-3Cu alloy by heat treatment, *Bioact. Mater.* 3 (1) (2018) 28–38, <https://doi.org/10.1016/j.bioactmat.2018.01.004>.
- [33] Z. Liu, S. Li, Z. Yin, Z. Zhu, L. Chen, W. Tan, Z. Chen, Stabilizing enzymes in plasmonic silk film for synergistic therapy of in situ SERS identified bacteria, *Adv. Sci.* 9 (6) (2022) e2104576, <https://doi.org/10.1002/advs.202104576>.
- [34] P. Gao, B. Fan, X. Yu, W. Liu, J. Wu, L. Shi, D. Yang, L. Tan, P. Wan, Y. Hao, S. Li, W. Hou, K. Yang, X. Li, Z. Guo, Biofunctional magnesium coated Ti6Al4V scaffold enhances osteogenesis and angiogenesis in vitro and in vivo for orthopedic application, *Bioact. Mater.* 5 (3) (2020) 680–693, <https://doi.org/10.1016/j.bioactmat.2020.04.019>.
- [35] R. Hashimoto, M. Minoshima, J. Kikuta, S. Yari, S.D. Bull, M. Ishii, K. Kikuchi, An acid-activatable fluorescence probe for imaging osteocytic bone resorption activity in deep bone cavities, *Angew. Chem., Int. Ed. Engl.* 59 (47) (2020) 20996–21000, <https://doi.org/10.1002/anie.202006388>.
- [36] A.B. Morris, C.R. Farley, D.F. Pinelli, L.E. Adams, M.S. Cragg, J.M. Boss, C.D. Scharer, M. Fribourg, P. Cravedi, P.S. Heeger, M.L. Ford, Signaling through the inhibitory fc receptor FcγRIIB induces CD8 T cell apoptosis to limit T cell immunity, *Immunity* 52 (1) (2020) 136–150, <https://doi.org/10.1016/j.immuni.2019.12.006>.